7-23-2018

Experimental and Computational Study of the (Z)-Selective Formation of Trisubstituted Olefins and Benzo-Fused Oxacycles from the Ruthenium-Catalyzed Dehydrative C–H Coupling of Phenols with Ketones

Hanbin Lee
Marquette University

Manoj V. Mane
Center for Catalytic Hydrocarbon Functionalizations

Ho Ryu
Korea Advanced Institute of Science and Technology (KAIST)

Debashis Sahu
Institute for Basic Science (IBS)

Mu-Hyun Baik
Institute for Basic Science (IBS)

See next page for additional authors

Journal of the American Chemical Society, Vol. 140, No. 32 (July 23, 2018): 10289-10296. DOI.

Experimental and Computational Study of the (*Z*)-Selective Formation of Trisubstituted Olefins and Benzo-Fused Oxacycles from the Ruthenium-Catalyzed Dehydrative C–H Coupling of Phenols with Ketones

Hanbin Lee

Department of Chemistry, Marquette University, Milwaukee, Wisconsin

Manoj V. Mane

Center for Catalytic Hydrocarbon Functionalizations, Institute for Basic Science (IBS), Daejeon 34141, Republic of Korea

Ho Ryu

Department of Chemistry, Korea Advanced Institute of Science and Technology (KAIST), Daejeon 34141, Republic of Korea

Debashis Sahu

Center for Catalytic Hydrocarbon Functionalizations, Institute for Basic Science (IBS), Daejeon 34141, Republic of Korea

Mu-Hyun Baik

Center for Catalytic Hydrocarbon Functionalizations, Institute for Basic Science (IBS), Daejeon 34141, Republic of Korea

Department of Chemistry, Korea Advanced Institute of Science and Technology (KAIST), Daejeon 34141, Republic of Korea

Chae S. Yi

Department of Chemistry, Marquette University, Milwaukee, Wisconsin

Abstract

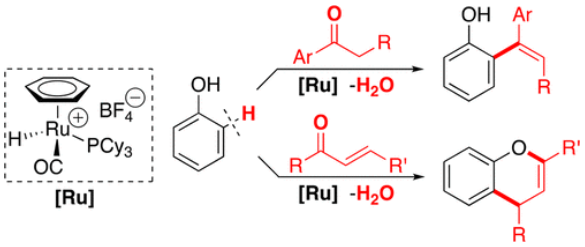

The cationic Ru–H complex was found to be an effective catalyst for the dehydrative C–H coupling of phenols with ketones to form the trisubstituted olefin products. The coupling of phenol with linear ketones led to highly stereoselective formation of the (*Z*)-olefin products. The dehydrative coupling of phenol with enones and diones efficiently formed the benzopyrene and related oxacyclic derivatives. The reaction of 3,5-dimethoxyphenol with cyclohexanone-2,2,6,6-d_4 showed a significant H/D exchange to both vinyl and α-CH_2 positions on the olefin product (72–75% D). A significant carbon isotope effect was observed on the *ortho*-arene carbon of the olefin product. The free energies of intermediate species for the entire catalytic cycle were successfully computed by using the DFT method. The DFT study revealed that the *E*/*Z* stereoselectivity is a result of the energy difference in the insertion step of *ortho*-metalated phenol to an enol form of the ketone substrate ($\Delta\Delta E$ = 9.6 kcal/mol). The coupling method provides a direct catalytic C–H olefination method for ketones to form trisubstituted olefins without employing any reactive reagents or forming any wasteful byproducts.

Introduction

Carbonyl olefination methods have long been considered as one of the most versatile C–C coupling protocols for the synthesis of complex organic molecules.(1) Traditionally, phosphorus ylide and related main group reagents have been widely used for the Wittig type of coupling reactions, but early transition metal reagents were also employed for McMurry(2) and Tebbe-Petasis(3) olefination reactions. Peterson olefination and related nucleophilic addition–elimination methods for aldehydes and ketones have also been successfully developed to

form substituted olefins.(1b,4) From the viewpoint of sustainable synthesis, these classical carbonyl olefination methods pose inherent drawbacks in that the usage of a stoichiometric amount of ylide or transition metal reagents results in the formation of a copious amount of toxic and wasteful byproducts. To overcome shortcomings associated with classical olefination methods, a concerted research effort in recent decades has been devoted to the development of strategies for catalytic carbonyl olefination. In a seminal work, Pd-catalyzed Negishi couplings of carbonyl derivatives with organozinc reagents have been extensively used for the synthesis of highly functionalized olefins and related molecules.(5) More recently, the Schindler group devised a remarkably effective intramolecular carbonyl-to-olefin metathesis reaction by using $FeCl_3$ as a catalyst.(6) Milstein and co-workers utilized pincer-ligated Ru catalysts to promote a selective carbonyl olefination via the coupling of alcohols with alkylsulfonates.(7) Zhou and co-workers cleverly designed a Ni-catalyzed olefination method from the coupling of arylketones with organoboron reagents.(8) Li recently reported a Ru-catalyzed carbonyl olefination method via hydrazine promoted reductive coupling of carbonyl compounds.(9) Despite such remarkable advances in designing catalytic olefination methods, these coupling methods still require reactive boron and sulfur reagents, which lead to the formation of salt byproducts. Additionally, they exhibit tendencies of undergoing undesired side reactions such as dehydrogenation and aldol-type condensation reactions. Catalytic C–H coupling methods have emerged as a step-efficient and direct olefination protocol for arenes,(10) although their synthetic utility has yet to be fully exploited in carbonyl olefination reactions.

One of the pertinent issues in carbonyl olefination methods has been concerned with controlling the stereochemistry of olefin products. In particular, designing (*Z*)-selective olefination methods has been considered the most challenging, since classical olefination methods generally favor the formation of (*E*)-olefins. In this regard, Peterson(4) and Horner–Wadsworth–Emmons(11) olefination methods have been extensively used for the synthesis of (*Z*)-olefin products, but the major issues on employing stoichiometric reagents and the formation of toxic byproducts have not been resolved for these methods. In terms of catalytic olefination methods, both Grubbs and Schrock-type metal-carbene catalysts have been successfully designed and utilized for a ring-closing metathesis reaction in forming biologically active (*Z*)-selective macrocyclic olefin products.(12) Pd-catalyzed Negishi-type coupling methods have also been successfully employed for the synthesis of (*Z*)-selective trisubstituted olefins.(5a)

We previously discovered that the cationic ruthenium hydride complex $[(C_6H_6)(PCy_3)(CO)RuH]^+BF_4^-$ (**1**) is a highly effective catalyst precursor for a number of dehydrative C–H coupling reactions of alkenes and arenes with alcohols.(13) Since these coupling reactions are driven by the formation of water, we reasoned that the analogous dehydrative C–H coupling reactions with carbonyl compounds might be feasible in achieving carbonyl olefination reactions. Herein, we report the scope and mechanistic study of ruthenium-catalyzed dehydrative coupling reaction of phenols with ketones, which leads to a highly (*Z*)-selective synthesis of trisubstituted olefin products. We combined experimental and computational analyses to establish a detailed mechanism as well as to elucidate the origin of stereoselectivity for the olefination reaction. The catalytic method features a direct catalytic C–H olefination method of ketones with phenols without employing any reactive reagents or forming any wasteful byproducts, while tolerating a number of common organic functional groups.

Results and Discussion

Reaction Scope

In an effort to extend the scope of dehydrative C–H coupling method of arenes,(13) we initially probed the feasibility of the coupling reaction of phenols with simple ketones by using the Ru–H catalyst. Thus, the treatment of 3,5-dimethoxyphenol (0.5 mmol) with propiophenone (1.0 mmol) in the presence of **1** (3 mol %) in 1,2-dichloroethane (2 mL) led to the formation of the alkenylated product (*Z*)-**2a** (eq 1). Among the screened catalysts, the Ru–H complex **1** exhibited distinctively high activity in forming the coupling product, as analyzed by both GC and NMR spectroscopic methods (Table S1, Supporting Information (SI)). Moreover, a highly stereoselective formation of (*Z*)-**2a** was observed, and its structure was unambiguously established by NMR spectroscopy (*vide infra*).

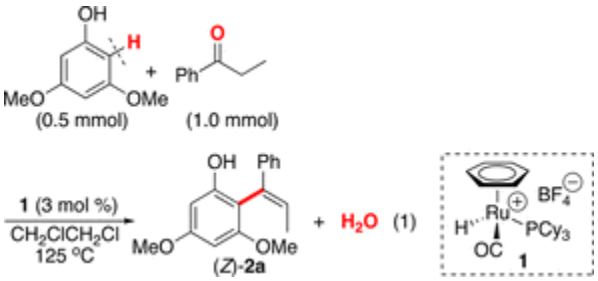

The substrate scope of the olefination reaction was explored using the catalyst **1**, as summarized in Table1. An electron-rich 3,5-dimethoxyphenol was found to be a suitable substrate for the coupling with aryl-substituted linear ketones to form *ortho*-alkenylated phenol products **2a**–**2n** (entries 1–14). For these aryl-substituted ketones, highly (*Z*)-selective olefin products **2a**–**2i** were formed in the crude mixture, as analyzed by GC-MS (entries 1–9). In contrast, the coupling with aliphatic linear ketones resulted in a mixture of (*E*)/(*Z*)-olefins, with the (*Z*)-isomer being the major products for **2k**–**2n** (entries 11–14). The analogous treatment of 3,5-dimethoxyphenol with cyclic ketones led to the clean formation of **2q**–**2s** (entries 17–19), while the coupling with 2-indanone yielded the indenyl-substituted product **2t** (entry 20). The coupling of 1-naphthol with linear and cyclic ketones led to the formation of the coupling products **2o** and **2v**, respectively (entries 15 and 22). The coupling reaction of phenols with an electron-withdrawing group was quite sluggish leading to low olefin product yields.

Table 1. Dehydrative C–H Olefination of Phenols with Ketones[a]

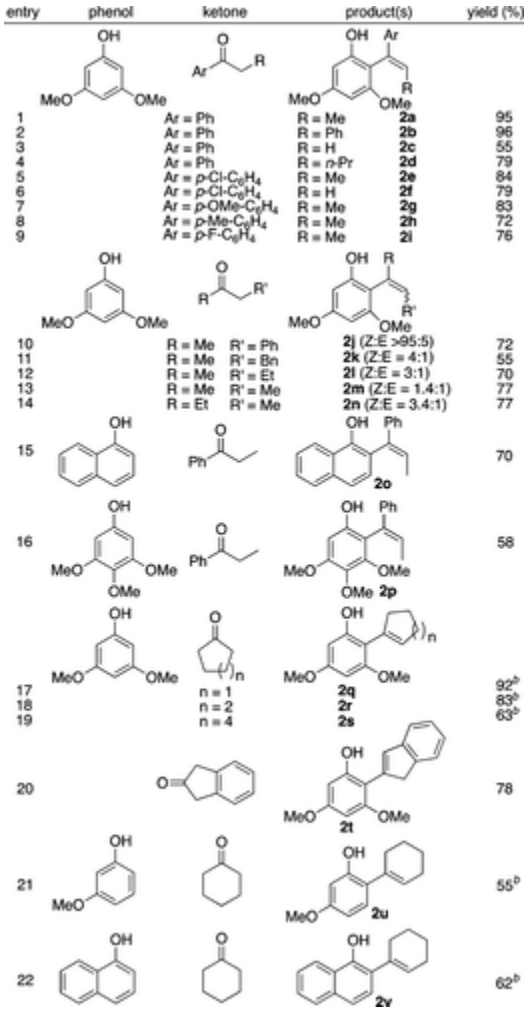

[a]Reaction conditions: phenol (0.5 mmol), ketone (1.0 mmol), 1,2-dichloroethane (2 mL), **1** (3 mol %), 125 °C, 16 h.
[b]1.5 mmol of ketone was used.

To further demonstrate its synthetic utility, we next surveyed the substrate scope of the catalytic carbonyl olefination method by employing a number of biologically active ketone substrates (Table2). Thus, the coupling of 3,5-dimethoxyphenol with 4-hydroxycoumarin yielded the coupling product **2w**, while the reaction with (+)-nootkatone led to the alkenylated product **2x** in a single step. Treatment with an anti-inflammatory agent nabumetone also readily afforded a 5:1 *Z*/*E* mixture of alkenylated product **2y**. Treatment with (+)-4-cholesten-3-one and adrenosterone predictively yielded the corresponding diene products **2z** and **2aa**, respectively.

Table 2. Dehydrative Coupling of 3,5-Dimethoxyphenol with Functionalized Ketones[a]

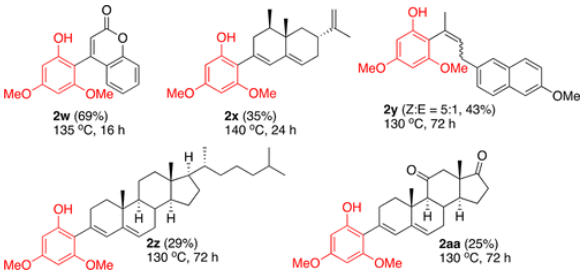

[a]Reaction conditions: phenol (0.5 mmol), ketone (1.0 mmol), 1,2-dichloroethane (2 mL), **1** (3 mol %).

The (*Z*)-stereochemistry of these olefin products was established by NMR spectroscopic methods. One of the most diagnostic features of the (*Z*)-olefin products is that allylic CH_2 protons of (*Z*)-**2** exhibited an ABX type of second-order pattern in the ^1H NMR spectrum due to a diastereotopic environment resulted from restricted rotation of the phenol group. In contrast, allylic CH_2 protons of (*E*)-**2** showed a simple first-order pattern. The stereochemistry of (*Z*)-**2a** was also definitively established by X-ray crystallography (Figure S3, SI). From both synthetic and environmental points of view, the salient features of the catalytic method are that it facilitates a direct C–H coupling of readily available phenol and ketone substrates in a highly regio- and stereoselective fashion and that it forms synthetically valuable trisubstituted olefin products **2** without using any reactive reagents or forming wasteful byproducts.

Computational Study

Inspired by related ruthenium-catalyzed dehydrative C–H coupling reactions, we initially compiled a plausible mechanistic pathway for the olefination reaction, which involves an initial *ortho*-C–H metalation of phenol, migratory insertion of the ketone substrate, and the subsequent dehydration and elimination steps (Scheme 1).(13a) However, despite our best efforts, we have not been able to detect or trap any catalytically relevant intermediate species, which made it difficult to establish a detailed mechanism of the coupling reaction experimentally. Thus, to attain deeper insights into the reaction mechanism and to elucidate the origin of (*E*)/(*Z*) selectivity, we turned to the DFT calculations. We have successfully computed the entire catalytic cycle for the coupling reaction of 3,5-dimethoxyphenol with 1,2-diphenylethanone substrates, and the free energy profile diagram has been constructed, as shown in Figure 1. The catalytic cycle begins with the Ru–H complex **1** forming a loosely bound transient adduct **4** with the phenol substrate, which can readily extrude the originally η^6-bound benzene ligand and proceed with the *ortho*-C–H metalation mediated by the phenolic OH directing group. The *ortho*-metalation step is associated with a barrier of 23.7 kcal/mol to generate the key intermediate complex **5**, which is only 5.1 kcal/mol uphill energetically, driven by the release of hydrogen gas (Figure S5, SI). As supporting experimental evidence for the benzene ligand dissociation, we previously observed a facile arene exchange reaction and the formation of free benzene from the coupling reactions mediated by the Ru–H catalyst **1**.(14)

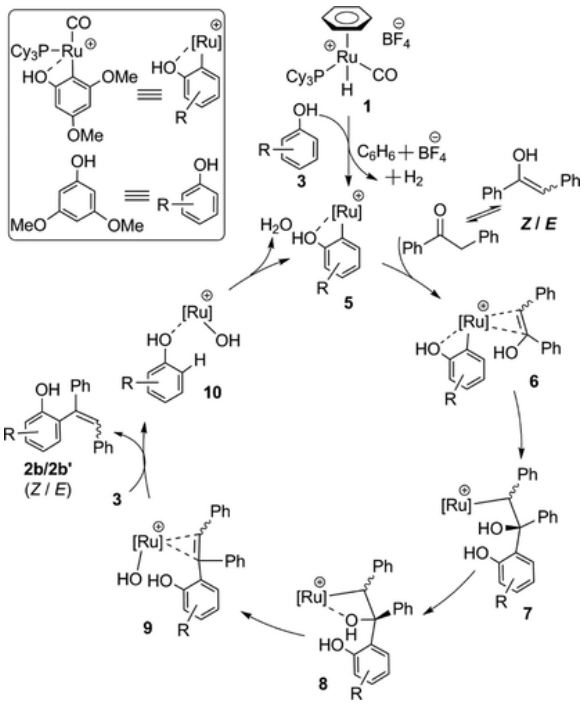

Scheme 1. Proposed Catalytic Cycle for the Coupling of 3,5-Dimethoxyphenol with 1,2-Diphenylethanone

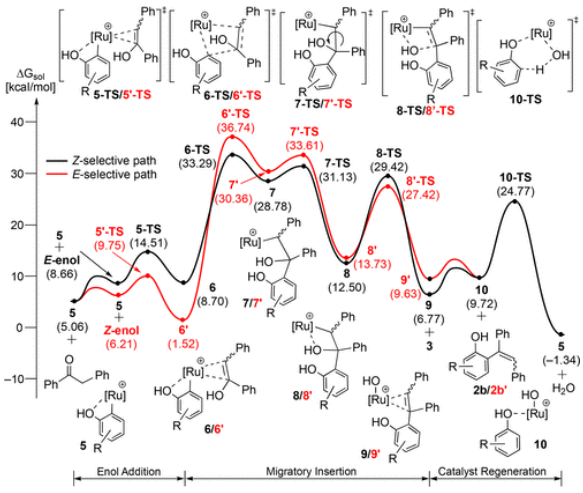

Figure 1. Free energy profile for the formation of (*E*)-**2b'** (red) and (*Z*)-**2b** (black) with water as the byproduct.

The intermediate **5** initiates the catalytic cycle by binding (*E*)- and (*Z*)-enol form of the ketone substrate to form the adducts **6** and **6'**, respectively. Interestingly, the adduct **6'** made by coordinating the (*Z*)-enol substrate is lower in energy by ∼7 kcal/mol than the analogue formed from (*E*)-enol substrate **6**. Subsequent migratory insertion affords intermediate **7**′ and **7** traversing via the transition state **6'-TS** and **6-TS**, where the relative energy between two stereoisomers is inverted during the migratory insertion step. At the transition state, the **6-TS** formed from the (*E*)-enol substrate is nearly 3.5 kcal/mol lower in energy than **6'-TS**, which contains the (*Z*)-enol substrate. This energy difference is notably diminished to ∼1.5 kcal/mol, but the relative ordering is maintained in the transient, high-energy intermediate **7** and **7**′. Rotation around the C–C bond leads to the much more stable intermediates **8** and **8'**, where the alkoxide group is appropriately positioned to act as a Lewis base and coordinated to the metal. The two diastereoisomers are predicted to be nearly isoenergetic at this intermediate state. To push the reaction forward, the hydroxyl group originating from the enol substrate must be eliminated via a dehydration step, as mentioned above. We explored several possible ways of accomplishing this task and found that the heterolytic cleavage of the C–OH bond accompanied by hydroxyl transfer to the Ru-center and reconstitution of the olefinic double bond of the substrate is energetically the most favorable pathway to give complex **9** and **9'**. Release of the product **2b** or **2b'** and addition of a new equivalent of phenol gives the ruthenahydroxyl-complex **10**, which can restart the catalytic cycle by activating the phenolic *ortho*-C–H bond and extruding an equivalent of water to generate intermediate **5**.

To understand the stereoselectivity described above, we performed a detailed fragment energy analysis on the migratory insertion step for both stereoisomers. In this analysis, we first fragment the intermediates **6**/**6'** and the transition states **6-TS**/**6'-TS** into chemically meaningful fragments, namely, the olefin substrate marked in blue and the ruthenium fragment carrying the ligands "**RuL**" as shown in red in Figure 2. Then, the energies of these fragments are calculated independently, which allows for evaluating how much energy is required to distort each of the fragments to the geometry found in the transition state.(15)Figure 2 summarizes the fragment and interaction energies, which can be computed by subtracting the sum of fragment energies from the total molecular energy. Interestingly, the majority of the energy difference between the two transition states is caused by the **RuL** fragment distortions. The **RuL** fragments in **6** must invest 17.2 kcal/mol to reach the

structure found in **6-TS**, whereas 24.7 kcal/mol must be invested to distort the structure of **RuL** in **6'** to what is found in **6'-TS**. This difference of 7.5 kcal/mol is by far the largest contributor to the electronic transition state energy difference of 9.6 kcal/mol. The olefin fragments require 25.3 and 26.1 kcal/mol energy, which is mostly invested into lengthening the C–C double bond in preparation of the migratory insertion. These distorted fragments interact with each other allowing recovery of 15.2 and 13.9 kcal/mol to afford the final transition state energies of 27.3 and 37.0 kcal/mol, as illustrated in Figure 2. It is curious that the interaction energy in **6-TS** is 1.3 kcal/mol greater although the fragment distortions are more severe in **6'-TS**. The degree of fragment distortion is generally related to the transition state being late, which means that both the bond breaking and bond forming processes should have progressed further. That is typically reflected in greater fragment distortion, but also in greater interaction energies.

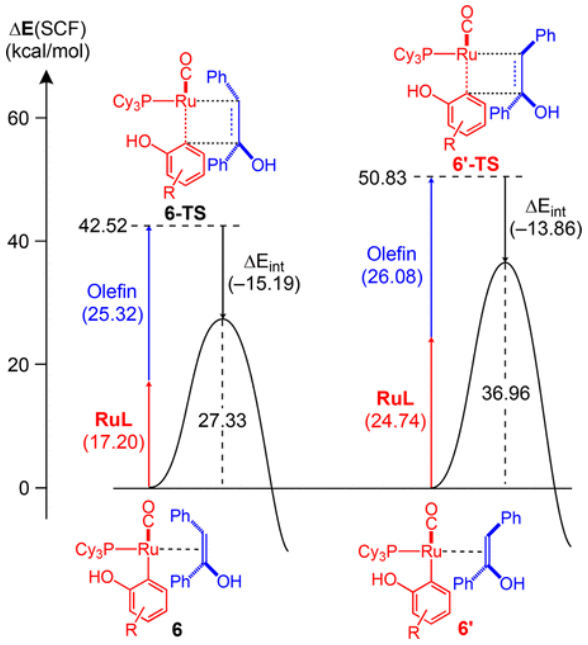

Figure 2. Fragment energy analysis of the migratory insertion step for the formation of (*Z*)-**2b** vs (*E*)-**2b**.

Figure 3 illustrates the structural difference between **6-TS** and **6'-TS**, which offers an explanation for the aforementioned energy components. In order to promote the insertion, the double bond between C2 and C3 must be broken, in conjunction with the formation of a new single bond between C1 and C2. The most relaxed geometry for this transition state features a square-planar metallacyclobutane-like structure. The **6-TS** adopts a fairly planar structure with the dihedral angle ∠Ru–C1–C2–C3 being ~5°, as shown in Figure 3a. In contrast, **6'-TS** has an unfavorable steric interaction between the phenyl group of the enol and the carbonyl group of the Ru-catalyst, which leads to a significant departure from planarity with the ∠Ru–C1–C2–C3 dihedral angle of ~26°, as illustrated in Figure 3b. The four bond lengths in the four-membered metallacycle directly report on how far the transition state has progressed away from the reactant state. The Ru–C1 bonds are 2.11 and 2.23 Å in **6-TS** and **6'-TS**, respectively, which is consistent with **6'-TS** being more distorted than **6-TS**, as discussed above. The C1–C2 bond is much longer at 2.17 Å in **6-TS** compared to 1.94 Å in **6'-TS**, again consistent with **6-TS** being an "earlier" transition state. The sterically induced deviation from planarity also explains why the interaction energy computed in the fragment energy analysis is notably diminished in **6'-TS**. As the π-orbitals from the olefin substrates and the in-plane d-orbitals on Ru cannot be optimally arranged due to the steric demand of the enol

in **6′-TS**, the interaction remains weak despite the larger structural distortion of each fragment, which is also a consequence of the steric clash between the carbonyl and the aromatic substituent on the enol.

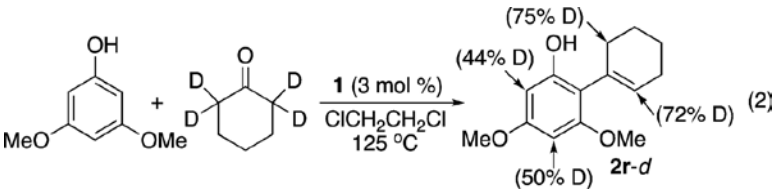

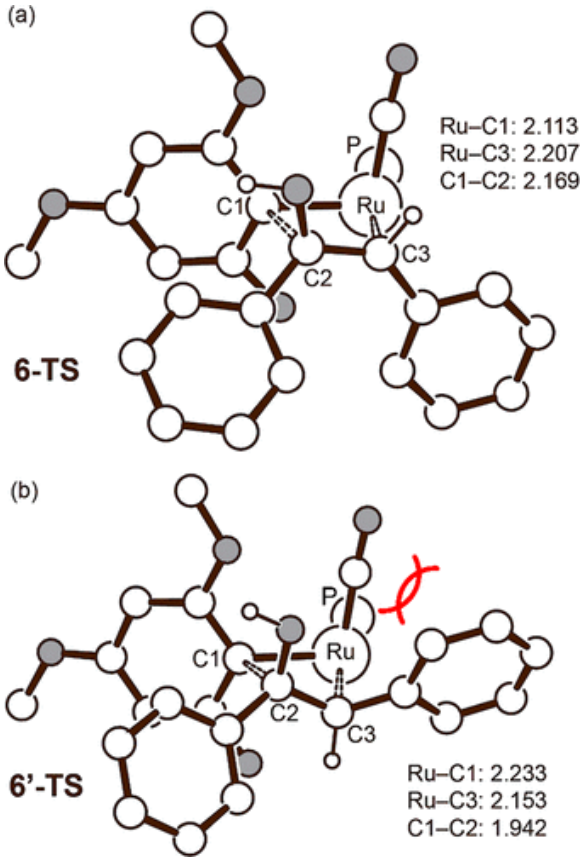

Figure 3. Optimized structures of the transition state (a) **6-TS** and (b) **6′-TS**. Oxygen atoms are shown in gray color. Nonessential atoms, such as the cyclohexyl groups on the phosphine ligand and nonessential hydrogen atoms, are not shown. Bond lengths are given in Å.

Experimental Support for the Mechanism

Several kinetic experiments were performed to assess the validity of the DFT computed mechanism. First, the H/D exchange pattern was examined from the reaction of 3,5-dimethoxyphenol with cyclohexanone-2,2,6,6-d_4 (93% D) (eq 2). The isolated product **2r**-*d* showed a significant amount of H/D exchange to both vinyl and α-CH_2 positions (72–75% D) as well as to the arene positions (Figure S1, SI). This H/D exchange pattern indicates a facile keto–enol tautomerization of the substrate under the reaction conditions. The extensive H/D exchange on the arene positions can readily be explained via the chelate assisted *ortho*-arene C–H metalation process; such a process has been well-known to occur rapidly and reversibly in metal-mediated coupling reactions via arene C–H activation.(16) To confirm the facile nature of the arene C–H activation step, the reaction rate was measured separately from the reaction of 3,5-dimethoxyphenol with cyclohexanone and cyclohexanone-2,2,6,6-d_4. A

negligibly small deuterium isotope effect of k_H/k_D = 1.1 ± 0.1 was obtained from the first-order rate plot (Figure S2, SI), again supporting the notion of a rapid and reversible arene C–H activation step for the coupling reaction.

As discussed above, our DFT calculations indicate that the migratory insertion of ketone substrate is the most likely rate-determining step. To confirm this computational result, we measured the carbon isotope effect from the coupling reaction of 3,5-dimethoxyphenol with propiophenone by employing Singleton's high-precision NMR technique (eq 3).(17) The most significant carbon isotope effect was observed on the *ortho*-arene carbon of the product (*Z*)-**2a** when the ^{13}C ratio of the product from a high conversion was compared with the sample obtained from a low conversion (^{13}C(avg 96% conversion)/^{13}C(avg 19% conversion) at C_{ortho} = 1.019; average of two runs) (Table S2, SI). No significant carbon isotope effect was observed on the carbonyl carbon, and this can be rationalized via an early asynchronous transition state of the multi-insertion steps as depicted in Figure 1.(18) Overall, the results are in good agreement with the calculated reaction energy profile as shown in Figure 1, further reinforcing that the C–C bond forming migratory insertion of the ketone substrate is the turnover-limiting step of the coupling reaction.

Synthetic Applications

These experimental and computational studies provided a new mechanistically driven rationale for designing stereoselective carbonyl olefination methods to construct biologically relevant structural motifs. In an effort to further extend its synthetic utility, we have begun to explore the dehydrative coupling method with enones and related carbonyl compounds (Scheme 2). For example, the coupling of 3,5-dimethoxyphenol with a linear enone 4-phenyl-3-buten-3-one led to the direct formation of chromene core structure **11**. In contrast, the coupling with a cyclic enone 2-cyclohexenone selectively yielded a bicyclic hemiketal product **12** with >95% diastereoselectivity. The molecular structure of **12** was definitively established by X-ray crystallography (Figure S4, SI). The couplings with 2-norbornanone and 2,5-hexanedione smoothly formed the bicyclic products **13** and **14**, respectively. These exploratory examples clearly demonstrate the synthetic power of dehydrative C–H coupling strategy in constructing oxygen heterocycle core structures without using any reactive reagents or forming toxic byproducts. We are currently pursuing to establish the scope of the coupling reactions between electron-rich arene substrates with these carbonyl compounds, and the results will be published in a separate article.

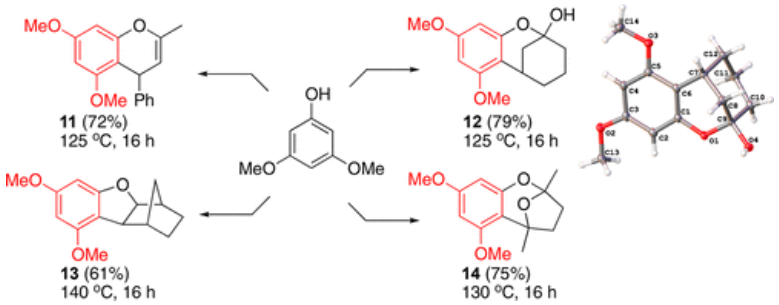

Scheme 2. Dehydrative Coupling of 3,5-Dimethoxyphenol with Ketones

Conclusions

In summary, we have successfully developed a highly chemo- and stereoselective dehydrative C–H olefination method of phenols with ketones to form trisubstituted olefins. The well-defined cationic ruthenium hydride catalyst was found to exhibit uniquely high activity and selectivity for promoting (*Z*)-olefin products. The experimental and computational studies provide a detailed mechanistic picture for the catalytic cycle, which consists of the *ortho*-metalation of phenol, migratory insertion of the carbonyl substrate, and dehydration steps in forming the olefin products. The DFT computational analysis revealed that the stereoselective formation of (*Z*)-olefins results from an unfavorable steric interaction between the substrate substituents and the axial carbonyl ligand of the Ru-catalyst during the migratory insertion step. The analogous C–H coupling reactions of enones and diones directly led to the formation of synthetically useful benzo-fused oxacyclic derivatives. Studies toward expanding the arene substrate scope as well as for exploiting mechanistic insights to increase synthetic applicability for this catalytic method are underway in our laboratories.

Experimental Section

General Information

All operations were carried out in a nitrogen-filled glovebox or by using standard high vacuum and Schlenk techniques unless otherwise noted. Solvents were freshly distilled over appropriate drying reagents. Benzene, toluene, and hexanes were distilled from purple solutions of sodium and benzophenone, and dichloromethane was dried over calcium hydride prior to use. All organic substrates were received from commercial sources and were used without further purification. Column chromatography was performed on Dynamic Absorbents silica gel 60A (32–63 μm particle size), and thin layer chromatography was performed on Agela TLC plates precoated with silica gel MF254. The NMR spectra were recorded on a Varian 300 or 400 MHz FT-NMR spectrometer, and the data are reported in parts per million (ppm) relative to TMS. Mass spectra were recorded from an Agilent 6850 GC-MS spectrometer with an HP-5 (5% phenylmethylpolysiloxane) column (30 m, 0.32 mm, 0.25 μm). High-resolution mass spectra (HRMS) were obtained at the Mass Spectrometry/ICP Lab, Department of Chemistry and Biochemistry, University of Wisconsin—Milwaukee, Milwaukee, WI. Elemental analyses were performed at the Midwest Microlab, Indianapolis, IN.

General Procedure for the Coupling Reaction of Phenol with Ketone

In a glovebox, a phenol (0.5 mmol), a ketone (1.0–1.5 mmol), and complex **1** (9 mg, 3 mol %) were dissolved in 1,2-dichloroethane (2 mL) in a 25 mL Schlenk tube equipped with a Teflon stopcock and a magnetic stirring bar. The tube was brought out of the glovebox and was stirred in an oil bath preset at 125–140 °C for 16–72 h. The reaction tube was taken out of the oil bath and was cooled to room temperature. After the tube was open to air, the solution was filtered through a short silica gel column by eluting with CH_2Cl_2 (10 mL), and the filtrate was analyzed by GC-MS. Analytically pure product was isolated by column chromatography on silica gel (230–460 mesh, hexanes/EtOAc). The product was completely characterized by NMR and GC-MS spectroscopic methods.

Computational Details

All calculations were carried out using DFT(19) as implemented in the Jaguar 9.1 suite(20) of *ab initio* quantum chemistry programs. Geometry optimizations were performed with the B3LYP(21) functional including Grimme's D3 dispersion correction(22) and the 6-31G** basis set. Ruthenium was represented using the Los Alamos LACVP basis(23) that includes effective core potentials. The energies of the optimized structures were reevaluated by additional single-point calculations on each optimized geometry using Dunning's correlation

consistent triple-ζ basis set cc-pVTZ(-f)(24) that includes a double set of polarization functions. For ruthenium, we used a modified version of LACVP, designated as LACV3P, in which the exponents were decontracted to match the effective core potential with triple-ζ quality. Solvation energies were evaluated by a self-consistent reaction field (SCRF)(25) approach based on accurate numerical solutions of the Poisson–Boltzmann equation. In the results reported, solvation calculations were carried out with the 6-31G**/LACVP basis at the optimized gas phase geometry employing the dielectric constant of ε = 10.36 for 1,2-dichloroethane. As is the case for all continuum models, the solvation energies are subject to empirical parametrization of the atomic radii that are used to generate the solute surface. We employed(26) the standard set of optimized radii in Jaguar for H (1.150 Å), C (1.900 Å), N (1.600 Å), P (2.074 Å), and Ru (1.481 Å). Analytical vibrational frequencies within the harmonic approximation were computed with the 6-31G**/LACVP basis to confirm proper convergence to well-defined minima or saddle points on the potential energy surface.

The energy components have been computed with the following protocol. The free energy in solution phase *G*(Sol) has been calculated as follows:

$$G(\text{Sol}) = G(\text{gas}) + G(\text{solv}) \quad (4)$$

$$G(\text{gas}) = H(\text{gas}) - TS(\text{gas}) \quad (5)$$

$$H(\text{gas}) = E(\text{SCF}) + \text{ZPE} \quad (6)$$

$$\Delta E(\text{SCF}) = \Sigma E(\text{SCF}) \text{ for products} - \Sigma E(\text{SCF}) \text{ for reactants} \quad (7)$$

$$\Delta G(\text{Sol}) = \Sigma G(\text{Sol}) \text{ for products} - \Sigma G(\text{Sol}) \text{ for reactants} \quad (8)$$

G(gas) is the free energy in gas phase; *G*(solv) is the free energy of solvation as computed using the continuum solvation model; *H*(gas) is the enthalpy in gas phase; *T* is the temperature (298.15 K); *S*(gas) is the entropy in gas phase; *E*(SCF) is the self-consistent field energy, i.e. “raw” electronic energy as computed from the SCF procedure; and ZPE is the zero-point energy. Note that by entropy here we refer specifically to the vibrational/rotational/translational entropy of the solute(s); the entropy of the solvent is incorporated implicitly in the continuum solvation model.

To locate transition states, the potential energy surface was first explored approximately using the linear synchronous transit (LST)(27) method, followed by a quadratic synchronous transit (QST)(28) search using the LST geometry as an initial guess.

Supporting Information

The Supporting Information is available free of charge on the ACS Publications website at DOI: 10.1021/jacs.8b05875.

- Experimental procedures, characterization data for organic products, and Cartesian coordinates of all computed structures and energy components (PDF)
- Crystallographic data for (*Z*)-**2a** (CIF)
- Crystallographic data for **12** (CIF)

- crystallographic information file
  - ja8b05875_si_002.cif (17.51 kb)
  - ja8b05875_si_003.cif (26.35 kb)
- pdf
  - ja8b05875_si_001.pdf (5.35 MB)

The authors declare no competing financial interest.

Acknowledgments

Financial support from the National Science of Foundation (CHE-1358439, CHE-1664652) and the National Institute of Health General Medical Science (R15 GM109273) is gratefully acknowledged. This research was supported in part by the Institute for Basic Science (IBS-R010-D1) in Korea.

References

1 (a) Maryanoff, B. E.; Reitz, A. B. The Wittig olefination reaction and modifications involving phosphoryl-stabilized carbanions. Stereochemistry, mechanism, and selected synthetic aspects. *Chem. Rev.* 1989, *89*, 863– 927, DOI: 10.1021/cr00094a007 (b) Flynn, A. B.; Ogilvie, W. W. Stereocontrolled Synthesis of Tetrasubstituted Olefins. *Chem. Rev.* 2007, *107*, 4698– 4745, DOI: 10.1021/cr050051k

2 (a) Fürstner, B. A.; Bogdanović, B. New developments in the chemistry of low-valent titanium. *Angew. Chem., Int. Ed. Engl.* 1996, *35*, 2442– 2469, DOI: 10.1002/anie.199624421 (b) Ephritikhine, M. New look at the McMurry reaction. *Chem. Commun.* 1998, 2549– 2554, DOI: 10.1039/a804394i (c) Takeda, T.; Tsubouchi, A. The McMurry Coupling and Related Reactions. *Org. React.* 2013, *82*, 1– 470, DOI: 10.1002/0471264180.or082.01

3 (a) Herrmann, W. A. The Methylene Bridge. *Adv. Organomet. Chem.* 1982, *20*, 159– 263, DOI: 10.1016/S0065-3055(08)60522-5 (b) Beadham, I.; Micklefield, J. Reagents for Carbonyl Methylenation in Organic Synthesis. *Curr. Org. Synth.* 2005, *2*, 231– 259, DOI: 10.2174/1570179053545396 (c) Hartley, R. C.; Li, J.; Main, C. A.; McKiernan, G. J. Titanium carbenoid reagents for converting carbonyl groups into alkenes. *Tetrahedron* 2007, *63*, 4825– 4864, DOI: 10.1016/j.tet.2007.03.015

4 (a) Chan, T.-H. Alkene Synthesis via β-Functionalized Organosilicon Compounds. *Acc. Chem. Res.* 1977, *10*, 442– 448, DOI: 10.1021/ar50120a003 (b) van Staden, L. F.; Gravestock, D.; Ager, D. J. New Developments in the Peterson Olefination Reaction. *Chem. Soc. Rev.* 2002, *31*, 195– 200, DOI: 10.1039/a908402i

5 (a) Negishi, E.; Huang, Z.; Wang, G.; Mohan, S.; Wang, C.; Hattori, H. Recent Advances in Efficient and Selective Synthesis of Di-, Tri-, and Tetrasubstituted Alkenes via Pd-Catalyzed Alkenylation–Carbonyl Olefination Synergy. *Acc. Chem. Res.* 2008, *41*, 1474– 1485, DOI: 10.1021/ar800038e (b) Hatakeyama, T.; Nakagawa, N.; Nakamura, M. Iron-Catalyzed Negishi Coupling Toward an Effective Olefin Synthesis. *Org. Lett.* 2009, *11*, 4496– 4499, DOI: 10.1021/ol901555r (c) Hu, F.; Xia, Y.; Ye, F.; Liu, Z.; Ma, C.; Zhang, Y.; Wang, J. Rhodium(III)-Catalyzedortho Alkenylation of N-Phenoxyacetamides with N-Tosylhydrazones or Diazoesters through C–H Activation. *Angew. Chem., Int. Ed.* 2014, *53*, 1364– 1367, DOI: 10.1002/anie.201309650

6 (a) Ludwig, J. R.; Zimmerman, P. M.; Gianino, J. B.; Schindler, C. S. Iron(III)-catalysed carbonyl–olefin metathesis. *Nature* 2016, *533*, 374– 379, DOI: 10.1038/nature17432 (b) Ludwig, J. R.; Phan, S.; McAtee, C. C.; Zimmerman, P. M.; Devery, J. J., III; Schindler, C. S. Mechanistic Investigations of the Iron(III)-Catalyzed Carbonyl-Olefin Metathesis Reaction. *J. Am. Chem. Soc.* 2017, *139*, 10832– 10842, DOI: 10.1021/jacs.7b05641

7 Srimani, D.; Leitus, G.; Ben-David, Y.; Milstein, D. Direct Catalytic Olefination of Alcohols with Sulfones. *Angew. Chem., Int. Ed.* 2014, *53*, 11092– 11095, DOI: 10.1002/anie.201407281

8 Lei, C.; Yip, Y. J.; Zhou, J. S. Nickel-Catalyzed Direct Synthesis of Aryl Olefins from Ketones and Organoboron Reagents under Neutral Conditions. *J. Am. Chem. Soc.* 2017, *139*, 6086– 6089, DOI: 10.1021/jacs.7b02742

9 Wei, W.; Dai, X.-J.; Wang, H.; Li, C.; Yang, X.; Li, C.-J. Ruthenium(II)-catalyzed olefination via carbonyl reductive cross-coupling. *Chem. Sci.* 2017, *8*, 8193– 8197, DOI: 10.1039/C7SC04207H

10 Recent reviews on C–H olefination: (a) Wencel-Delord, J.; Dröge, T.; Liu, F.; Glorius, F. Towards mild metal-catalyzed C–H bond activation. *Chem. Soc. Rev.* 2011, *40*, 4740– 4761, DOI: 10.1039/c1cs15083a . (b) Arockiam, P. B.; Bruneau, C.; Dixneuf, P. H. Ruthenium(II)-Catalyzed C–H Bond Activation and Functionalization. *Chem. Rev.* 2012, *112*, 5879– 5918, DOI: 10.1021/cr300153j (c) Kozhushkov, S. I.; Ackermann, L. Ruthenium-catalyzed direct oxidative alkenylation of arenes through twofold C–H bond functionalization. *Chem. Sci.* 2013, *4*, 886– 896, DOI: 10.1039/C2SC21524A (d) Yeung, C. S.; Dong, V. M. Catalytic Dehydrogenative Cross-Coupling: Forming Carbon–Carbon Bonds by Oxidizing Two Carbon–Hydrogen Bonds. *Chem. Rev.* 2011, *111*, 1215– 1292, DOI: 10.1021/cr100280d

11 (a) Stec, W. J. Wadsworth-Emmons reaction revisited. *Acc. Chem. Res.* 1983, *16*, 411– 417, DOI: 10.1021/ar00095a004 (b) Patois, C.; Savignac, P.; About-Jaudet, E.; Collignon, N. Bis(Trifluoroethyl)(Carboethoxymethyl)Phosphonate. *Org. Synth.* 1996, *73*, 152– 155, DOI: 10.15227/orgsyn.073.0152

12 (a) Hansen, E. C.; Lee, D. Efficient and Z-Selective Cross-Metathesis of Conjugated Enynes. *Org. Lett.* 2004, *6*, 2035– 2038, DOI: 10.1021/ol049378i (b) Ibrahem, I.; Yu, M.; Schrock, R. R.; Hoveyda, A. H. Highly Z- and Enantioselective Ring-Opening/Cross-Metathesis Reactions Catalyzed by Stereogenic-at-Mo Adamantylimido Complexes. *J. Am. Chem. Soc.* 2009, *131*, 3844– 3845, DOI: 10.1021/ja900097n (c) Rosebrugh, L. E.; Herbert, M. B.; Marx, V. M.; Keitz, B. K.; Grubbs, R. H. Highly Active Ruthenium Metathesis Catalysts Exhibiting Unprecedented Activity and Z-Selectivity. *J. Am. Chem. Soc.* 2013, *135*, 1276– 1279, DOI: 10.1021/ja311916m (d) Mann, T. J.; Speed, A. W. H.; Schrock, R. R.; Hoveyda, A. H. Catalytic Z-Selective Cross-Metathesis with Secondary Silyl- and Benzyl-Protected Allylic Ethers: Mechanistic Aspects and Applications to Natural Product Synthesis. *Angew. Chem., Int. Ed.* 2013, *52*, 8395– 8400, DOI: 10.1002/anie.201302538

13 (a) Lee, D.-H.; Kwon, K.-H.; Yi, C. S. Dehydrative C–H Alkylation and Alkenylation of Phenols with Alcohols: Expedient Synthesis for Substituted Phenols and Benzofurans. *J. Am. Chem. Soc.* 2012, *134*, 7325– 7328, DOI: 10.1021/ja302710v (b) Kim, J.; Lee, D.-H.; Kalutharage, N.; Yi, C. S. Selective Catalytic Synthesis of Unsymmetrical Ethers from the Dehydrative Etherification of Two Different Alcohols. *ACS Catal.* 2014, *4*, 3881– 3885, DOI: 10.1021/cs5012537 (c) Lee, H.; Yi, C. S. Catalytic Synthesis of Substituted Indoles and Quinolines from the Dehydrative C–H Coupling of Arylamines with 1,2- and 1,3-Diols. *Organometallics* 2016, *35*, 1973– 1977, DOI: 10.1021/acs.organomet.6b00273 (d) Kim, J.; Pannilawithana, N.; Yi, C. S. Catalytic Tandem and One-Pot Dehydrogenation–Alkylation and – Insertion Reactions of Saturated Hydrocarbons with Alcohols and Alkenes. *ACS Catal.* 2016, *6*, 8395– 8398, DOI: 10.1021/acscatal.6b02186

14 (a) Lee, D. W.; Yi, C. S. Chain-Selective and Regioselective Ethylene and Styrene Dimerization Reactions Catalyzed by a Well-Defined Cationic Ruthenium Hydride Complex: New Insights on the Styrene Dimerization Mechanism. *Organometallics* 2010, *29*, 3413– 3417, DOI: 10.1021/om100468q (b) Kim, J.; Yi, C. S. Intermolecular Markovnikov-Selective Hydroacylation of Olefins Catalyzed by a Cationic Ruthenium–Hydride Complex. *ACS Catal.* 2016, *6*, 3336– 3339, DOI: 10.1021/acscatal.6b00856

15 (a) Xie, S.; Lopez, S. A.; Ramström, O.; Yan, M.; Houk, K. N. 1,3-Dipolar Cycloaddition Reactivities of Perfluorinated Aryl Azides with Enamines and Strained Dipolarophiles. *J. Am. Chem. Soc.* 2015, *137*, 2958– 2966, DOI: 10.1021/ja511457g (b) Ess, D. H.; Houk, K. N. Theory of 1,3-Dipolar Cycloadditions: Distortion/Interaction and Frontier Molecular Orbital Models. *J. Am. Chem. Soc.* 2008, *130*, 10187– 10198, DOI: 10.1021/ja800009z (c) Ess, D. H.; Houk, K. N. Distortion/Interaction Energy Control of 1,3-Dipolar Cycloaddition Reactivity. *J. Am. Chem. Soc.* 2007, *129*, 10646– 10647, DOI: 10.1021/ja0734086

16 (a) Kakiuchi, F.; Murai, S. Catalytic C–H/Olefin Coupling. *Acc. Chem. Res.* 2002, *35*, 826– 834, DOI: 10.1021/ar960318p (b) Kakiuchi, F.; Kochi, T.; Mizushima, E.; Murai, S. Room-Temperature Regioselective C–H/Olefin Coupling of Aromatic Ketones Using an Activated Ruthenium Catalyst with a Carbonyl Ligand and Structural Elucidation of Key Intermediates. *J. Am. Chem. Soc.* 2010, *132*, 17741– 17750, DOI: 10.1021/ja104918f

17 (a) Singleton, D. A.; Thomas, A. A. High-Precision Simultaneous Determination of Multiple Small Kinetic Isotope Effects at Natural Abundance. *J. Am. Chem. Soc.* 1995, *117*, 9357– 9358, DOI: 10.1021/ja00141a030 (b) Frantz, D. E.; Singleton, D. A.; Snyder, J. P. ^{13}C Kinetic Isotope Effects for the Addition of Lithium Dibutylcuprate to Cyclohexenone. Reductive Elimination Is Rate-Determining. *J. Am. Chem. Soc.* 1997, *119*, 3383– 3384, DOI: 10.1021/ja9636348 (c) Nowlan, D. T., III; Gregg, T. M.; Davies, H. M. L.; Singleton, D. A. Isotope Effects and the Nature of Selectivity in Rhodium-Catalyzed Cyclopropanations. *J. Am. Chem. Soc.* 2003, *125*, 15902– 15911, DOI: 10.1021/ja036025q

18 Nowlan, D. T., III; Singleton, D. A. Mechanism and Origin of Enantioselectivity in the $Rh_2(OAc)(DPTI)_3$-Catalyzed Cyclopropenation of Alkynes. *J. Am. Chem. Soc.* 2005, *127*, 6190– 6191, DOI: 10.1021/ja0504441

19 Parr, R. G.; Yang, W. *Density Functional Theory of Atoms and Molecules*; Oxford University Press: New York, 1989.

20 Bochevarov, A. D.; Harder, E.; Hughes, T. F.; Greenwood, J. R.; Braden, D. A.; Philipp, D. M.; Rinaldo, D.; Halls, M. D.; Zhang, J.; Friesner, R. A. Jaguar: A high-performance quantum chemistry software program with strengths in life and materials sciences. *Int. J. Quantum Chem.* 2013, *113*, 2110– 2142, DOI: 10.1002/qua.24481

21 (a) Slater, J. C. *Quantum Theory of Molecules and Solids, Vol. 4: The Self-Consistent Field for Molecules and Solids*; McGraw-Hill: New York, 1974. (b) Vosko, S. H.; Wilk, L.; Nusair, M. Accurate spin-dependent electron liquid correlation energies for local spin density calculations: a critical analysis. *Can. J. Phys.* 1980, *58*, 1200– 1211, DOI: 10.1139/p80-159 (c) Becke, A. D. Density-functional exchange-energy approximation with correct asymptotic behavior. *Phys. Rev. A: At., Mol., Opt. Phys.* 1988, *38*, 3098– 3100, DOI: 10.1103/PhysRevA.38.3098 (d) Lee, C.; Yang, W.; Parr, R. G. Development of the Colle-Salvetti correlation-energy formula into a functional of the electron density. *Phys. Rev. B: Condens. Matter Mater. Phys.* 1988, *37*, 785– 789, DOI: 10.1103/PhysRevB.37.785 (e) Becke, A. D. Density-functional thermochemistry. III. The role of exact exchange. *J. Chem. Phys.* 1993, *98*, 5648– 5652, DOI: 10.1063/1.464913

22 Grimme, S.; Antony, J.; Ehrlich, S.; Krieg, H. A consistent and accurate ab initio parametrization of density functional dispersion correction (DFT-D) for the 94 elements H-Pu. *J. Chem. Phys.* 2010, *132*, 154104, DOI: 10.1063/1.3382344

23 (a) Hay, P. J.; Wadt, W. R. Ab initio effective core potentials for molecular calculations. Potentials for the transition metal atoms Sc to Hg. *J. Chem. Phys.* 1985, *82*, 270– 283, DOI: 10.1063/1.448799 (b) Wadt, W. R.; Hay, P. J. Ab initio effective core potentials for molecular calculations. Potentials for main group elements Na to Bi. *J. Chem. Phys.* 1985, *82*, 284– 298, DOI: 10.1063/1.448800 (c) Hay, P. J.; Wadt, W. R. Ab initio effective core potentials for molecular calculations. Potentials for K to Au including the outermost core orbitals. *J. Chem. Phys.* 1985, *82*, 299– 310, DOI: 10.1063/1.448975

24 Dunning, T. H., Jr. Gaussian basis sets for use in correlated molecular calculations. I. The atoms boron through neon and hydrogen. *J. Chem. Phys.* 1989, *90*, 1007– 1023, DOI: 10.1063/1.456153

25 (a) Marten, B.; Kim, K.; Cortis, C.; Friesner, R. A.; Murphy, R. B.; Ringnalda, M. N.; Sitkoff, D.; Honig, B. New Model for Calculation of Solvation Free Energies: Correction of Self-Consistent Reaction Field Continuum Dielectric Theory for Short-Range Hydrogen-Bonding Effects. *J. Phys. Chem.* 1996, *100*, 11775– 11788, DOI: 10.1021/jp953087x (b) Edinger, S. R.; Cortis, C.; Shenkin, P. S.; Friesner, R. A. Solvation Free Energies of Peptides: Comparison of Approximate Continuum Solvation Models with Accurate Solution of the Poisson–Boltzmann Equation. *J. Phys. Chem. B* 1997, *101*, 1190– 1197, DOI: 10.1021/jp962156k (c) Friedrichs, M.; Zhou, R.; Edinger, S. R.; Friesner, R. A. Poisson–Boltzmann Analytical Gradients for Molecular Modeling Calculations. *J. Phys. Chem. B* 1999, *103*, 3057– 3061, DOI: 10.1021/jp982513m

26 Rashin, A. A.; Honig, B. Reevaluation of the Born model of ion hydration. *J. Phys. Chem.* 1985, *89*, 5588– 5593, DOI: 10.1021/j100272a006

27 Halgren, T. A.; Lipscomb, W. N. The synchronous-transit method for determining reaction pathways and locating molecular transition states. *Chem. Phys. Lett.* 1977, *49*, 225– 232, DOI: 10.1016/0009-2614(77)80574-5

28 Peng, C. Y.; Schlegel, H. B. Combining Synchronous Transit and Quasi-Newton Methods to Find Transition States. *Isr. J. Chem.* 1993, *33*, 449– 454, DOI: 10.1002/ijch.199300051